JOURNAL OF MATERIALS SCIENCE 15 (1980) 2559–2568

Co-precipitated RuO_2–Al_2O_3 catalysts: bulk and surface characterization

F. GARBASSI, A. BOSSI, G. PETRINI
Istituto Guido Donegani S.p.A. Via Fauser, 4-28100 Novara, Italy

A series of co-precipitated RuO_2–Al_2O_3 samples was characterized by means of bulk and surface techniques such as X-ray diffraction (XRD), specific surface area measurements, X-ray photoelectron spectroscopy (XPS) and Auger electron spectroscopy (AES). The existence of a substitutional solid solution of Al^{3+} ions in RuO_2 is suggested on the basis of XRD results. A more detailed study of such a phase was hindered by its thermal instability. XPS and AES quantitative data indicate a strong enrichment of Al on the surface. A simple model based on a reciprocal masking action of the particles of the two oxides with respect to the primary beam (X-rays or electrons) was found to fit the surface composition data well.

1. Introduction

Supported metal catalysts are a class of materials in which considerable interest has grown in recent years [1]. The most widely used preparation technique of such materials is the impregnation of a preformed support (typically an oxide or high area carbon) with a solution of a proper metal compound. Some strong limitations are implied in this preparation method, concerning for example the achievement of the required metal content in the final product and its uniformity of distribution in the porous structure of the support [2]. If a high metal content is required (generally more than 10%) and the support is a stable oxide such as silica or alumina, a co-precipitation procedure can be adopted. Reduction of the product gives an intimate mixture of metallic and oxide particles. Ni-containing catalysts prepared in this way are widely used in the methanation reaction [3]. As a part of the study on ruthenium supported catalysts [4, 5], a series of co-precipitated ruthenium dioxide–alumina samples with a wide range of compositions were prepared. This paper deals with the bulk and surface characterization of the samples, before reduction, mainly by X-ray diffraction (XRD), specific surface area measurements, X-ray photoelectron spectroscopy (XPS) and Auger electron spectroscopy (AES).

2. Experimental procedures

Samples were prepared by pouring ammonia while stirring into a diluted solution containing the necessary amount of $Al(NO_3)_3 \cdot 9H_2O$ (C. Erba) and commercial ruthenium trichloride (Rudi Pont) at 333 K and until pH 8 was reached. After filtering and washing with water, the precipitates were dried at 383 K and fired at several temperatures (573 to 1073 K) for 20 h. The ruthenium content in the dried solids was determined by atomic absorption spectroscopy. In the following, the samples are indicated by the abbreviation Rxyz, where xyz corresponds to the weight percent of RuO_2 in each co-precipitate.

X-ray diffraction patterns were obtained using a Philips 1050/25 powder diffractometer using Cu$K\alpha$ radiation. The same samples were examined in a PHI (Physical Electronics Industries) LEED-AES-XPS system, recording both the X-ray photoelectron and Auger spectra after inserting the powder in an In foil [6]. The spectrometer was connected to a PDP 11/50 computer (Digital Corp.) for data collection. The pressure in the analysis chamber was maintained at less than 2×10^{-7} Pa during the experiments. XP spectra of O 1s, Al 2p, Ru 3p and Ru 3d transitions were collected at a pass energy of 50 eV, using the Mg$K\alpha$ radiation at a power of 400 W. Each peak

0022–2461/80/102559–10 $03.00/0

was an average of 10 to 30 scans, depending on its intensity. The Ru $3p_{3/2}$ peak was chosen for the quantitative surface analysis because of the overlap of the C 1s contamination peak on the strongest Ru 3d doublet. Intensities were determined by numerical integration after subtracting the background contribution. This last was obtained drawing a baseline tangent to the base on both sides of each peak, provided that background steps due to inelastic secondary electrons appeared negligible. Atomic ratios were determined by correcting the respective intensity I for the photoelectric cross-sections

$$\frac{N_x}{N_y} = \frac{I_x}{I_y}\frac{\sigma_y}{\sigma_x},$$

using the σ values previously calculated by Scofield [7]. Auger analyses were carried out at a primary energy of 3 KeV and a current of 30 μA, at a modulation voltage of 3 V peak-to-peak. In this case, atomic ratios were calculated by correcting the respective peak heights H for the empirical sensitivity factors [8]. Ru($M_5N_{2,3}N_{4,5}$), O($KL_{2,3}L_{2,3}$) and Al(KL_3L_3) peak heights were measured. The above mentioned Ru transition was preferred to the stronger Ru($M_5N_{4,5}N_{4,5}$) being free from the overlapping of the C(KL_1L_1) contamination peak. An argon ion gun operating at a voltage of 1 KV and a pressure of 7×10^{-3} Pa was occasionally used for depth profiling experiments.

Surface area values were determined by N_2 adsorption at 77 K using a Carlo Erba Sorptomatic Series 1800 instrument.

3. Results and discussion

3.1. *Structural characterization*

After drying at 383 K, α-$Al_2O_3 \cdot H_2O$ (boehmite) was the only crystalline phase detected by XRD. Heating in air at 673 K determined the appearance of γ-Al_2O_3, together with RuO_2 peaks. The more intense peaks, (1 1 0), (1 0 1) and (2 1 1) appeared distorted on the higher angles side. The distortion decreased by increasing the heating temperature and practically disappeared at 1073 K. At the same temperature the $\gamma \rightarrow \alpha$-$Al_2O_3$ transition occurred, which is normally observed at $T \geqslant 1373$ K [9]. In Fig. 1, the (1 0 1) peak profiles of RuO_2 in the sample R019 are reported versus temperature in the range 673 to 1073 K. Such a distortion was not observed in the XRD spectra of pure RuO_2, pure γ-Al_2O_3 (both prepared by precipitation) or

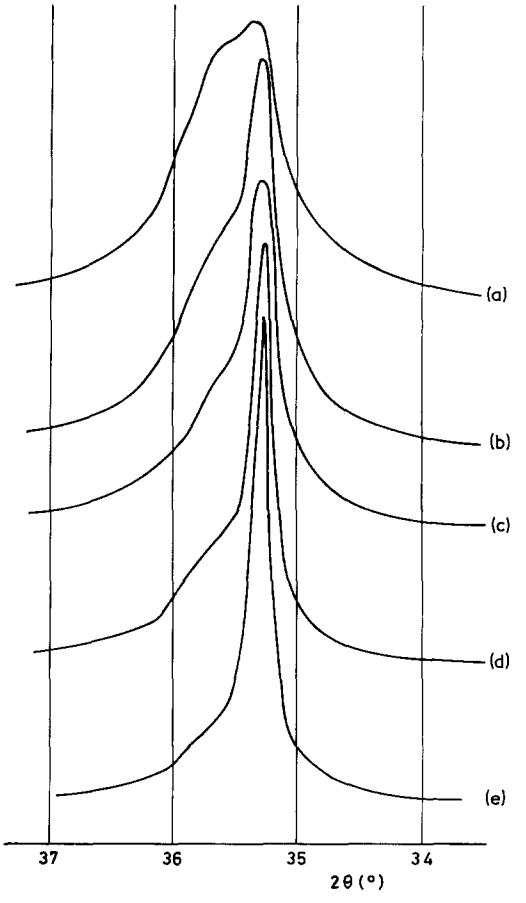

Figure 1 X-ray diffraction profile of 1 0 1 peak of sample R019 after heating at different temperatures (a) 673 K; (b) 773 K; (c) 873 K; (d) 973 K; (e) 1073 K).

their mechanical mixtures heating in the same temperature range. The distorted peak profiles were deconvoluted into two components, one at the right ruthenia angular position, and the other at higher angles. The angular difference $\Delta\alpha$ of the two resulting peaks was found to be quite insensitive to temperature, while a slight decrease was observed with an increase of Ru content (Fig. 2). On the contrary, the intensity ratio P, between the component at higher angles and the RuO_2 one, depends strongly on temperature, but not on composition (Fig. 3). We suggest that the diffraction peak at higher angles is due to the insertion of Al^{3+} ions into the RuO_2 structure, probably through an amorphous precursor formed during co-precipitation. This can occur in different ways, resulting in an interstitial or substitutional solid solution.

The first hypothesis, that is, the insertion of aluminium ions into the tetrahedral hollows present

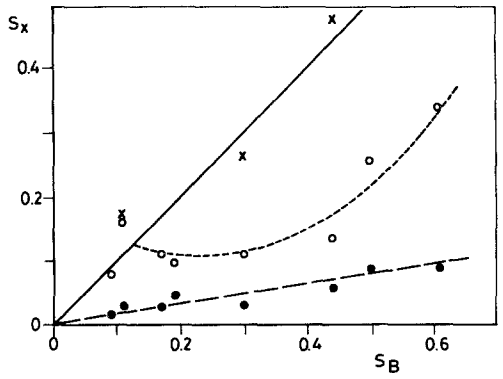

Figure 2 $\Delta\alpha_{101}$ angular difference between the two components of RuO_2 diffraction peak versus bulk composition expressed as Ru/Al atomic ratio (○: 773 K; ×: 873 K; ●: 973 K).

in the rutile structure of ruthenia [10] can be envisaged dimensionally (Al^{3+} ionic radius; 0.51 Å [11]), but can be ruled out by examining the peak intensity ratios. In fact, such an insertion must cause a variation in the relative intensities of the diffraction peaks with respect to those of RuO_2. Actually, this was not observed.

The formation of a substitutional solid solution is consistent with the shrinking of d-spacings. Obviously, the substitution of Ru^{4+} ions with Al^{3+} should be accompanied by oxygen vacancies in order to maintain the electrical neutrality. Similar defect structures were found in titania–alumina coated photoanodes [12]. The poor dependence of $\Delta\alpha$ on composition (Fig. 2) indicates a narrow existence field of the solid solution, while its thermal instability suggests that the foreign ions are easily expelled from the ruthenia lattice.

As pointed out above, the γ-$Al_2O_3 \rightarrow \alpha$-$Al_2O_3$ transformation was observed at a temperature noticeably lower than normally [9]. A similar lowering of the phase transition temperature was observed when γ-alumina supporting Pt particles was heated at 1123 K in vacuum or in H_2 [13]. Such a decrease was attributed to the presence of Pt or to hydrogen in the surrounding atmosphere. As in the present investigation the transition was observed after heating in air, the solid solution is likely to be involved in such a phenomenon. It can be suggested that at the interface with alumina, the Al^{3+} ions expelled from the rutile structure activate the formation of the corundum phase. This subject remains open to future investigation.

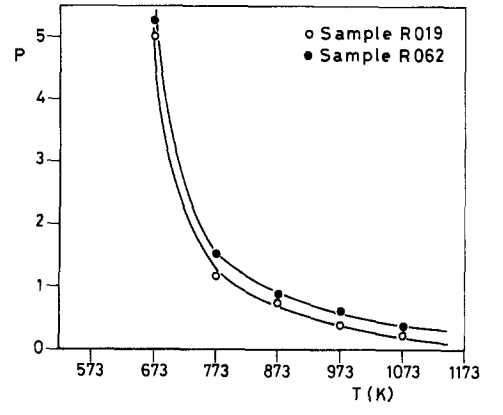

Figure 3 Intensity ratio between the high angle and low angle components of RuO_2 (1 0 1) diffraction peak versus temperature at two different compositions.

3.2. Morphological characterization

The experimental specific surface area values are shown in Figs. 4 and 5 as a function of composition and heating treatment respectively. All data were found to fit the following equation well

$$Q = [A(1-x_1)+B(1-x_2)] \exp(-C/RT) \quad (1)$$

where Q is the calculated specific area (m^2g^{-1}), x_1 and x_2 the weight fractions of RuO_2 and Al_2O_3 respectively, R the gas constant (1.986 cal. $mole^{-1}K^{-1}$) and T the temperature. A correlation factor of 0.997 and a standard deviation of 9.15 were found for the best fit. The calculated curves, plotted in Figs. 4 and 5, show a good consistency of the model, particularly at specific surface area values greater than 100 m^2g^{-1}. The best fitting coefficients are $A = 43.95$, $B = 3.15$ and $C = -2531.5$ (cal mol^{-1}).

For every composition the total specific surface area of the co-precipitate appears as the linear combination of the pure components surface areas treated at the same temperature, suggesting that the interaction between the two oxides observed by XRD does not have a strong influence on the morphology of the particles.

3.3. Surface characterization

Ru/Al atomic ratios, obtained by XPS and AES analyses on samples treated at various temperatures are reported in Tables I and II respectively, where S_X indicate the XPS result, S_A the AES result and S_B the bulk atomic ratio. On samples heated at a temperature between 573 K and 973 K, S_X follows S_B up to a value of ~ 0.15, then shows a broad minimum, remaining well below the correspondent bulk ratio. On samples heated at 1073 K

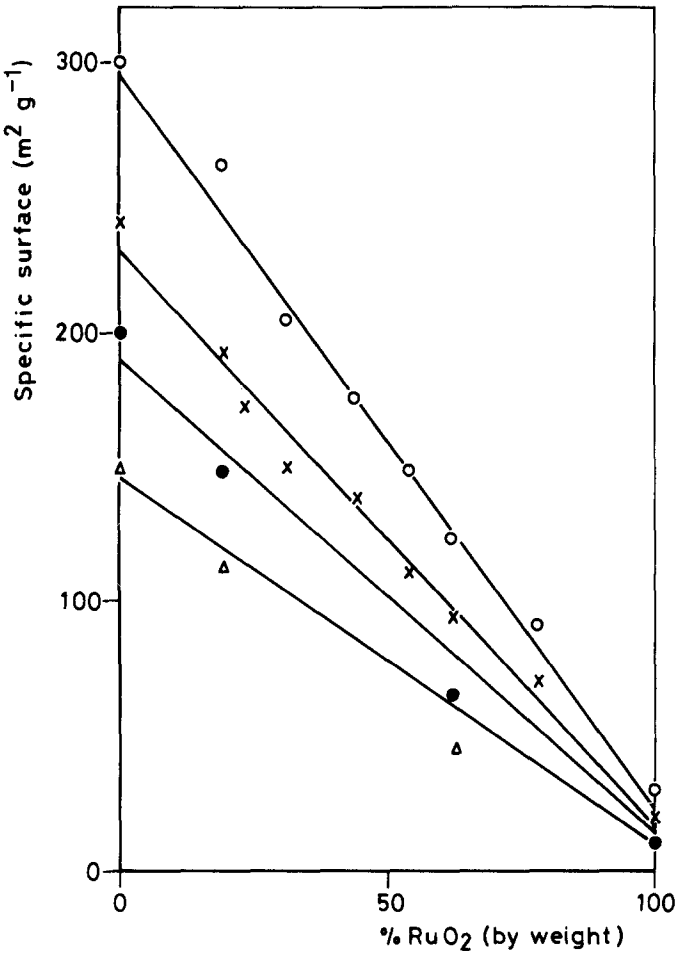

Figure 4 Specific surface area versus composition at several heating temperatures (○: 673 K; × : 773 K; ●: 873 K; △: 1073 K). Straight lines represent the best fit obtained by Equation 1.

a linear trend occurs, with S_X values lower than the previous ones. A comparison of results obtained on samples calcined at 973 K or 1073 K is reported in Fig. 6. Similar results were obtained by AES, as it is shown in Fig. 7.

Since the methods used in drawing the surface compositions do not allow the data to be considered as having an absolute significance, but only a relative value, obtaining comparable results by two different techniques is meaningful. In other words, strong matrix effects on the photoelectric cross-section values (for XPS) or on the elemental sensitivity factors (for AES) can be excluded. Beam damage effects in the AES mode were not observed by repeating the collection of the Auger spectra on the same region of samples.

Some samples were subjected to ion etching for 60 min. New S_X values approaching those of the bulk were found on samples previously having an Al content on the surface higher than that expected on the basis of their bulk composition (Fig. 6). Even if a preferential sputtering effect cannot be *a priori* excluded, this result strongly supports the existence of an effective Al enrichment and the accuracy of the analysis. As the etching rate of the ion gun employed is about 15 Å min^{-1} in the adopted experimental conditions (measured bombarding a Ta_2O_5 film of known thickness), it is also apparent that the Al enrichment is not limited to some surface layers, but maintained to a large depth.

An attempt to use mechanical mixtures of RuO_2 and γ-Al_2O_3 as external standards was found unsuitable, since the alumina particles "coated" ruthenia during the powder mixing, resulting in samples in which Ru was almost undetectable.

3.4. Interpretation of surface composition data

The interpretation of surface composition data on the basis of a physical model depends on the

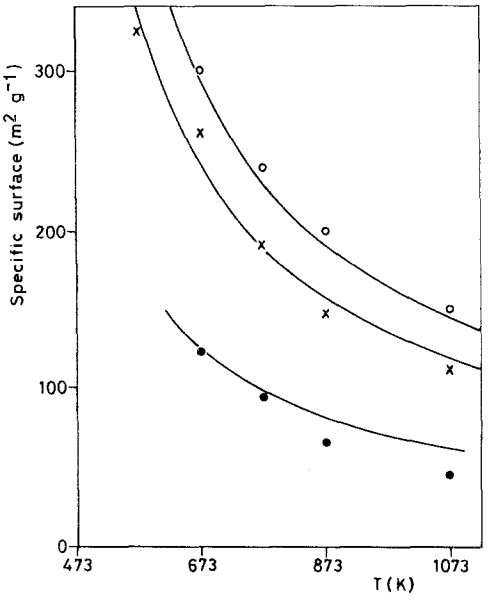

Figure 5 Specific surface area versus temperature for several compositions (○: sample R000; ×: sample R019; ●: sample R062). Curves represent the best fit obtained by Equation 1.

complexity of the system under investigation. The simplest and most studied case is that of binary alloys [14]. It is however necessary to study equilibrated samples [15] and the sample morphology was found to affect the surface composition [16].

On ternary systems, there is little data available in the literature. A model of non-stoichiometric cobalt ferrite was developed which fits the behaviour of the surface composition versus bulk cationic ratio quite well [17, 18]. In this system, the presence of a single phase simplifies the theoretical approach. A monotonic correspondence was found between surface and bulk composition in co-precipitated $NiO-Al_2O_3$ catalysts. Good agreement was also found between the experimental data and the calculated curve [19]. The authors discussed their results in terms of the influence of particle size of NiO over the range of studied compositions.

The dependence of the surface composition on the bulk composition in the $RuO_2-Al_2O_3$ system is rather more complex. Assuming a strong influence of morphology on the experimental results, a simple model was elaborated which allowed calculation of the Ru/Al atomic ratios, S_c, as a function of the average particle radii R and r of RuO_2 and Al_2O_3 respectively and of the escape depth δ of the photoemitted electrons.

This model is based on the assumption that the composition observed by a surface sensitive technique is the result of a reciprocal masking action of the particles of the two oxides with respect to the primary beam (X-rays or electrons). This action essentially depends on particle size and the relative quantity of each oxide. Details on the elaboration of the model are reported in the Appendix.

The following relation was found

$$S_c = \frac{mxr^2}{2MyR^2} \times \frac{4rV(xd + yD) - 3(drx + DRy)}{4Rv(xd + yD) - 3(drx + DRy)}, \quad (2)$$

where V and v are functions of R, r and δ. Other quantities are physical constants or depend on the given composition. A sensitivity test for the model is also reported in the Appendix. Equation 2 was found to be weakly sensitive to R, r, δ and composition, while a strong and complex dependence on the R/r ratio occurs. An infinite number of (R, r) couples satisfy the condition $S_c = S_X$ (or S_A). With the aim of correlating R and r to the experimental system, the total specific surface area values Q were taken into account. Assuming a spherical shape for particles and considering Q as the sum of the surface areas of the two oxides

TABLE I Ru/Al atomic ratios from XPS data

Sample	S_B	S_X (573 K)	S_X (773 K)	S_X (873 K)	S_X (973 K)	S_X (1073 K)
R019	0.09	0.05	0.05	0.06	0.08	0.02
R023	0.11	–	0.12	0.11	0.16	0.03
R031	0.17	0.08	0.15	0.10	0.11	0.03
R033	0.19	–	0.11	0.06	0.10	0.05
R044	0.30	0.07	0.10	0.06	0.11	0.03
R054	0.44	0.16	0.07	0.12	0.14	0.06
R057	0.50	–	0.12	0.13	0.26	0.09
R062	0.61	0.31	0.20	0.19	0.34	0.09
R078	1.33	–	0.32	–	–	–
R090	3.44	–	0.64	–	–	–

TABLE II Ru/Al atomic ratios from AES data

Sample	S_B	S_A (773 K)	S_A (873 K)	S_A (973 K)	S_A (1073 K)
R019	0.09	0.16	0.12	0.09	0.05
R023	0.11	0.14	0.17	0.16	0.06
R031	0.17	0.17	0.17	0.17	0.05
R033	0.19	0.15	0.19	0.18	0.08
R044	0.30	0.08	0.17	0.09	0.05
R054	0.44	0.16	0.26	0.09	0.06
R057	0.50	0.14	0.27	0.22	0.11
R062	0.61	0.30	0.35	0.28	0.11
R078	1.33	0.44	–	–	–
R090	3.44	1.35	–	–	–

$$\text{particle radius} = \frac{K}{\text{density} \times \text{surface area}}, \quad (3)$$

where the particle radius is measured in Å and K is a constant of value 3×10^4, R and r can be set in such a way as to obtain

$$K\left(\frac{x}{DR} + \frac{y}{dr}\right) = Q. \quad (4)$$

As some experimental Q values were not available, values calculated according to Equation 1 were used. Results of calculations on a series of samples with different compositions heated at 773 K and at a particular composition heated at various temperatures are collected in Table III and shown in Fig. 8. Errors were determined assuming an uncertainty of ± 5% in S_X and Q.

Nearly constant r values in the whole range of compositions were obtained from Equation 2, while R (and consequently R/r) follows a non-monotonic trend. In fact, its reasonable tendency to increase with the content of RuO_2 has two exceptions, at the left side of the plot and at intermediate compositions, where a maximum is present. The first situation probably depends on the low value of S_X at 773 K (see Table I) with respect to those found at higher temperatures and compositions. By imposing $S_X = S_B$, an R value of 40 Å should be obtained, aligned with the nearest ones. The observed maximum is connected with the minimum in the S_X–S_B plot, suggesting that the co-precipitation conditions in that range bring forth large ruthenia particle sizes. Taking into account the experimental results and Equation 1, specific surface areas near 20 and 230 $m^2\ g^{-1}$ are expected for ruthenia and alumina respectively on heating at 773 K. From Equation 4, R and r values corresponding to surface areas of 13 to 120 $m^2\ g^{-1}$ and 200 to 235 $m^2\ g^{-1}$ respectively were found (Table III). Thus, calculated r values are in excellent agreement with specific surface area measurements.

Calculated specific surfaces of RuO_2 indicate a dispersion effect due to co-precipitation at the highest ruthenia dilutions. Such high values ought to cause a deviation from linearity in total specific area values. On the contrary, this was not observed (Fig. 4). However, contributions of RuO_2 to the total specific area at this side of the composition range are limited by its low content, as one can see taking into account the weight fraction x (right column of Table III): a maximum contribution of 28 $m^2\ g^{-1}$ is derived from the R values, corresponding to deviations from linearity of 15 to 20 $m^2\ g^{-1}$. Such small variations can be partially confused into the experimental error.

Also the growing effect caused by temperature is satisfactorily described by the model. As reported in Fig. 9, a slow and parallel increase in particle size of both oxides occurs with increasing temperature, in accordance with expectations, with a sharp variation of R between 873 K and 1073 K.

It must be pointed out that the system under

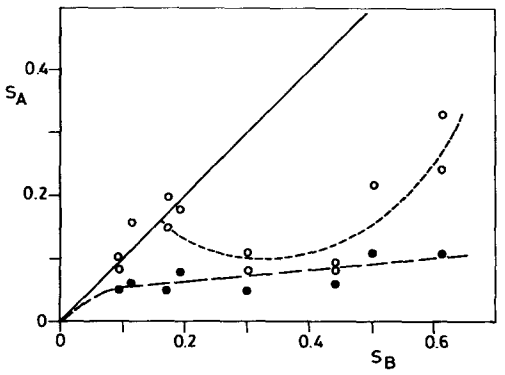

Figure 6 S_X versus bulk composition; ○: samples heated at 973 K; ×: the same after 60 min. of ion bombardment; ●: samples heated at 1073 K.

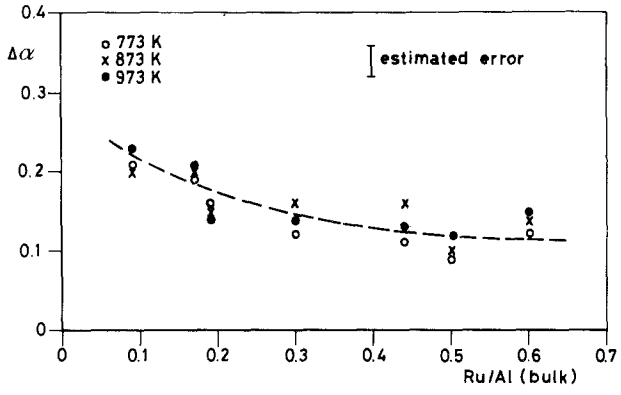

Figure 7 S_A versus bulk composition for samples heated at 973 K (○) and 1073 K (●).

examination is not the most suitable for an in depth study of a morphological model, since an independent method for checking particle sizes of both oxides is not available. In fact, specific surface area measurements give results which are the sum of different phase contributions. X-ray broadening methods can be applied only to RuO_2 peaks, since those of alumina are too weak and distorted by overlaps. Moreover, an accurate application to RuO_2 is complicated by the deformation of such peaks. However, using the Scherrer formula [20] particle radii between 80 and 150 Å

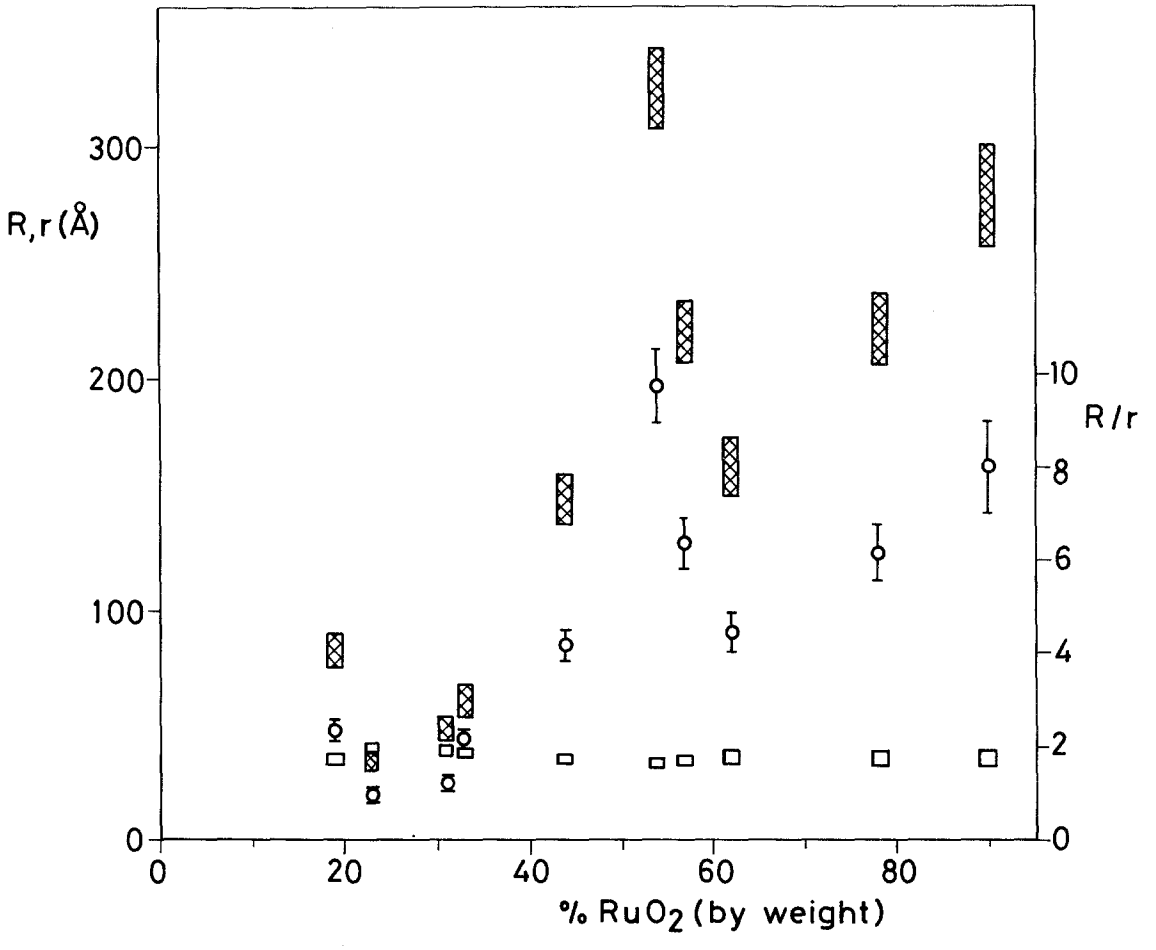

Figure 8 R (full bars) and r (empty bars) calculated values from Equation 2 versus bulk composition for samples heated at 773 K. Bar lengths indicate the variations corresponding to a ± 5% uncertainty of S_X and Q. R/r values are also reported (open circles).

TABLE III Calculated S_C values from Equation 2

Sample	T(K)	r(Å)	R(Å)	R/r	Al_2O_3 surface area ($m^2\ g^{-1}$)	RuO_2 surface area ($m^2\ g^{-1}$)	
					(1)	(1)	(2)
R019	773	35 ± 2	82 ± 7	2.3 ± 0.3	220	52	10
R023	773	38.5 ± 2.5	35.5 ± 5	0.9 ± 0.2	200	121	28
R031	773	39 ± 2	47.5 ± 4.5	1.2 ± 0.1	197	90	28
R033	773	37 ± 2	79.5 ± 7	2.2 ± 0.2	208	54	18
R044	773	35 ± 2	147 ± 10	4.2 ± 0.4	220	29	13
R054	773	33 ± 2	324 ± 17	9.8 ± 0.8	233	13	7
R057	773	34 ± 2	218 ± 13	6.4 ± 0.5	226	20	11
R062	773	36 ± 2.5	161 ± 12	4.5 ± 0.5	214	27	17
R078	773	35.5 ± 2.5	220 ± 15	6.2 ± 0.6	217	19	15
R090	773	34.5 ± 3.5	278 ± 21	8.1 ± 1.0	223	15	13
R019	573	19.5 ± 1	63.5 ± 3.5	3.3 ± 0.3	394	67	13
R019	873	43.5 ± 2	77 ± 7	1.8 ± 0.2	177	56	11
R019	1073	53.5 ± 2.5	303 ± 32	5.7 ± 0.7	144	14	3

(1) Calculated surface area of the single oxide from Equation 3 in the text.
(2) Calculated contribution of RuO_2 to the total surface area of the sample.

were found increasing with composition, not far from R values, and in a simple relationship with them (Fig. 10).

4. Conclusions

1) After a thermal treatment at 573 K of co-precipitated RuO_2–Al_2O_3 samples, a three phases mixture was obtained: ruthenia, γ-alumina and a rutile-structure phase with cell parameters smaller and closer to RuO_2.

2) This phase is unstable and disappears on increasing the heating temperature. It is likely to be a substitutional solid solution of Al^{3+} ions in the lattice of ruthenium dioxide.

3) The surface composition of co-precipitated samples shows a remarkable Al enrichment; the behaviour of the surface Ru/Al ratio versus bulk Ru/Al shows a broad minimum.

4) A simple morphological model was elaborated where the surface composition behaviour is related to a masking effect of alumina particles on ruthenia particles with respect to the surface sensitive probe (AES or XPS).

5) The existence of an interaction between the

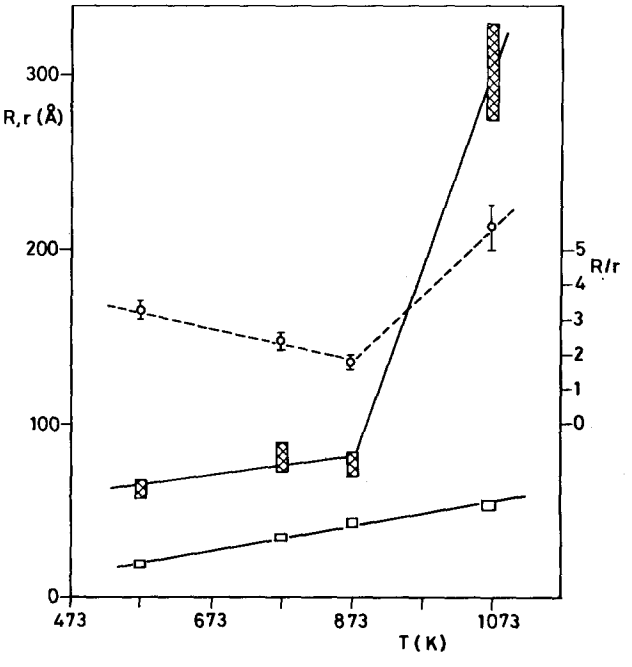

Figure 9 R (full bars) and r (empty bars) calculated values from Equation 2 versus heating temperature for sample R019. Bar lengths indicate the variations corresponding to a ± 5% uncertainty of S_X and Q. R/r values are also reported (open circles).

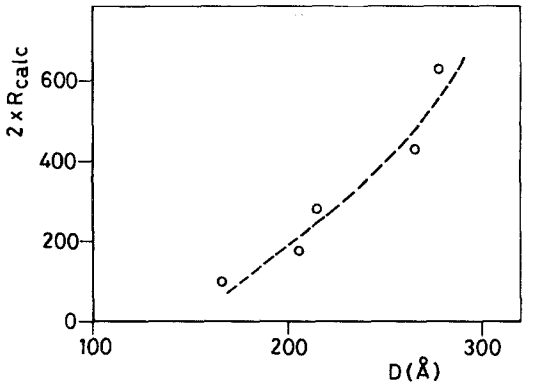

Figure 10 Calculated R values from Equation 2 (multiplied by 2) versus crystallite size D from XRD analysis.

two oxides makes the co-precipitated samples interesting from the point of view of heterogeneous catalysis. The study of the same system after reduction and the comparison of its activity and selectivity with supported Ru/Al_2O_3 catalysts prepared traditionally will be the further steps of this investigation.

Acknowledgements

We are grateful for the technical assistance of Mr. L. Pozzi (XPS and AES data), Mr. V. Bozzola (X-ray diffraction data) and Mr. R. Berté (specific surface area measurements). We are also indebted to Prof. J. C. J. Bart and Prof. S. Pizzini for valuable discussions and interest in this work.

Appendix

Given D, R and x, the density, average particles radius and weight fraction of RuO_2 in each co-precipitated sample, and d, r and y, the same quantities of Al_2O_3, the number of RuO_2 or Al_2O_3 particles per gram of sample will be

$$\frac{3x}{4\pi DR^3} \tag{A1}$$

and

$$\frac{3y}{4\pi dr^3}. \tag{A2}$$

Assuming that each alumina particle is able to mask a surface of area πr^2, and the average escape depth is δ (as a matter of fact, a lower escape depth value should be assumed for Ru transitions with respect to Al ones, both in XPS and AES mode), the total volume masked by all alumina particles will be

$$\pi r^2 \delta \frac{3y}{4\pi r^3 d} = \frac{3y\delta}{4rd}. \tag{A3}$$

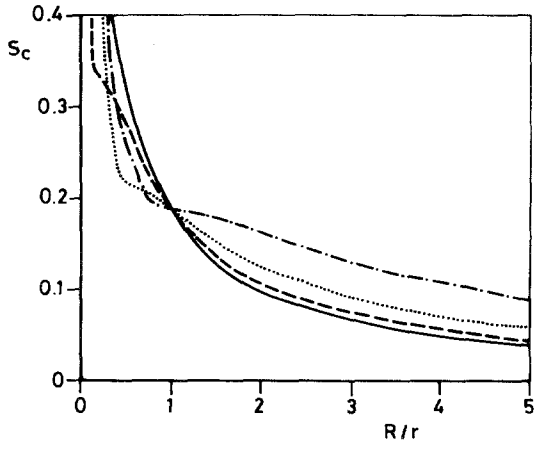

Figure 11 S_C versus R/r at different r values (——— $r = 120$ Å; – – – $r = 60$ Å; . . . . . $r = 30$ Å; –·– $r = 15$ Å).

Similarly, the total volume masked by RuO_2 particles is

$$\frac{3x\delta}{4DR}. \tag{A4}$$

Taking into account the volume fraction present for each oxide

$$\frac{xd}{xd + yD} = a \tag{A5}$$

and

$$\frac{yD}{xd + yD} = b, \tag{A6}$$

for ruthenia and alumina respectively, the fraction of masked particles for each oxide will be

$$RuO_2: \frac{3\delta a}{4}\left(\frac{x}{DR} + \frac{y}{dr}\right) = \eta_R \tag{A7}$$

and

$$Al_2O_3: \frac{3\delta b}{4}\left(\frac{x}{DR} + \frac{y}{dr}\right) = \eta_A. \tag{A8}$$

For each particle, the analysed volumes will be

$$\frac{4\pi V}{3} \tag{A9}$$

or

$$\frac{4\pi v}{3}, \tag{A10}$$

for ruthenia or alumina respectively, where V and v correspond to

$$R^3 - (R-\delta)^3 \text{ and } r^3 - (r-\delta)^3.$$

The analysed volume for all particles in 1 g of sample will be, from Equations A1, A2, A9 and A10

$$\frac{xV}{DR^3} \text{ and } \frac{yv}{dr^3},$$

without considering the mutual masking action. If this effect is considered, a correction must be applied taking into account Equations A7 and A8:

$$\frac{XV}{DR^3} - \eta_R \quad (\text{for } RuO_2),$$

$$\frac{yv}{dr^3} - \eta_A \quad (\text{for } Al_2O_3).$$

If M and m are the respective molecular weights of the oxides, the same relationship, proportional to the number of Ru or Al atoms, can be expressed as

$$\left(\frac{xV}{DR^3} - \eta_R\right)\frac{D}{M} \quad (\text{for } RuO_2) \qquad (A11)$$

and

$$\left(\frac{yv}{dr^3} - \eta_A\right)\frac{2d}{m} \quad (\text{for } Al_2O_3). \qquad (A12)$$

Elaborating and taking the ratio of the two expressions, a Ru/Al $= S_c$ relation is obtained

$$S_c = \frac{mxr^2}{2MyR^2}\,\frac{4rV(xd + yD) - 3(drx + DRy)}{4Rv(xd + yD) - 3(drx + DRy)}. \qquad (A13)$$

From Equation A13, for each (x, y) composition we can choose R and r values in such a way to obtain

$$S_c = S_x \,(\text{or } S_A).$$

Equation 13 was obtained by considering 1 g of sample analysed using a surface technique in which primary beam and analysed particles (these last with an escape depth δ) impinge on and are emitted off into the whole three-dimensional space. Actually, in commercial Auger or photoemission spectrometers, a primary beam of limited diameter is used, and the emitted electrons are collected in a small solid angle region.

We assume that these limitations do not strongly affect the ratio expressed by Equation A13. Another simplification used is that an array of spheres of equal diameter cannot completely mask a surface (actually, about 7% of it remains free).

The sensitivity of the model described by Equation A13 was tested with respect to various parameters, i.e. r, R, R/r, and composition.

A moderate and monotonic dependence of S_c on δ and composition was found, at different R and r values. Thus the choice of an average escape depth value or a 10% uncertainty in the bulk experimental composition do not critically affect the present results. Instead, the dependence on R/r is strong, quite independently from imposed R and r values. As an example, in Fig. 11, the behaviour of S_c versus R/r is reported for several r values as in the case of the sample R033. In the case of $r = R$, S depends on composition only, as is apparent by the form of Equation A13. A slow decrease with the increase of R/r occurs when $R > r$, while for $R < r$ a more complicated relation was found.

References

1. D. P. BURKE, *Chem. Week*, (March 28, 1979) p. 42 and (April 4, 1979) p. 46.
2. J. P. ANDERSON, "Structure of metallic catalysts" (Academic Press, New York and London, 1975).
3. R. L. MOSS, in "Experimental Methods in Catalytic Research", Vol. 2, edited by R. B. Anderson and P. T. Dawson (Academic Press, New York and London, 1976).
4. F. GARBASSI, A. BOSSI, A. ORLANDI, G. PETRINI and L. ZANDERIGHI, *Ned. Tijdsch. Vacuumtechn.* **16** (1978) 35.
5. A. BOSSI, F. GARBASSI, A. ORLANDI, G. PETRINI and L. ZANDERIGHI, in "Preparation of Catalysts II", edited by B. Delman, P. Grange, P. Jacobs and G. Poncelet (Elsevier, Amsterdam, 1979) p. 405.
6. G. E. THERIAULT, T. L. BARRY and M. J. B. THOMAS, *Anal. Chem.* 47 (1975) 1492.
7. J. M. SCOFIELD, *J. Electron Spectrosc. Relat. Phenom* 8 (1976) 129.
8. P. W. PALMBERG, *Anal. Chem.* **45** (1973) 549A.
9. K. WEFERS and G. M. BELL, "Oxides and Hydroxides of Aluminum", Alcoa Technical Paper No. 19 (1972).
10. R. W. G. WYCKOFF, "Crystal Structures" Vol. I (Interscience, New York, 1960).
11. R. C. WEAST, ed., "Handbook of Chemistry and Physics" 55th edn (CRC Press, Cleveland, 1974) p. F-198.
12. J. AUGUSTYNSKI, J. HINDEN and C. STALDER, *J. Electrochem. Soc.* **124** (1977) 1063.
13. Y. F. CHU and E. RUCKENSTEIN, *J. Catal.* **55** (1978) 281.
14. S. H. OVERBURY, P. A. BERTRAND and G. A. SOMORJAI, *Chem. Rev.* 75 (1975) 547.
15. F. GARBASSI and G. PARRAVANO, *Surface Sci.* 71 (1978) 42.
16. J. A. SCHWARTZ, R. S. POLIZZOTTI and J. J. BURTON, *ibid.* 67 (1977) 429.
17. F. GARBASSI, G. PETRINI, L. POZZI, G. BENEDEK and G. PARRAVANO, *ibid.* 68 (1977) 286.
18. G. BENEDEK, F. GARBASSI, G. PETRINI and G. PARRAVANO, *J. Phys. Chem. Solids* 39 (1978) 637 and 645.
19. R. B. SHALVOY and P. J. REUCROFT, *J. Electron Spectrosc. Relat. Phenom.* **12** (1977) 351.
20. H. P. KLUG and L. E. ALEXANDER, "X-ray Diffraction Procedures" (John Wiley & Sons, New York, 1959) p. 512.

Received 24 September and accepted 10 March 1980.